DOI: 10.1002/ejic.201001118

Supramolecular Approach to Gold Nanoparticle/Triruthenium Cluster Hybrid Materials and Interfaces

Sergio H. Toma,[a] Jonnatan J. Santos,[a] Koiti Araki,*[a] and Henrique E. Toma[a]

Keywords: Gold / Ruthenium / Nanoparticles / Cluster compounds / Raman spectroscopy

A systematic and comprehensive study of the interaction of citrate-stabilized gold nanoparticles with triruthenium cluster complexes of general formula $[Ru_3(CH_3COO)_6(L)]^+$ [L = 4-cyanopyridine (4-CNpy), 4,4′-bipyridine (4,4′-bpy) or 4,4′-bis(pyridyl)ethylene (bpe)] has been carried out. The cluster–nanoparticle interaction in solution and the construction of thin films of the hybrid materials were investigated in detail by electronic and surface plasmon resonance (SPR) spectroscopy, Raman scattering spectroscopy and scanning electron microscopy (SEM). Citrate-stabilized gold nanoparticles readily interacted with $[Ru_3O(CH_3COO)_6(L)_3]^+$ complexes to generate functionalized nanoparticles that tend to aggregate according to rates and extents that depend on the bond strength defined by the characteristics of the cluster L ligands following the sequence bpe > 4,4′-bpy >> 4-CNpy. The formation of compact thin films of hybrid AuNP/$[Ru_3O(CH_3COO)_6(L)_3]^+$ derivatives with L = bpe and 4,4′-bpy indicated that the stability/lability of AuNP–cluster bonds as well as their solubility are important parameters that influence the film contruction process. Fluorine-doped tin oxide electrodes modified with thin films of these nanomaterials exhibited similar electrocatalytic activity but much higher sensitivity than a conventional gold electrode in the oxidation of nitrite ion to nitrate depending on the bridging cluster complex, demonstrating the high potential for the development of amperometric sensors.

Introduction

In recent years, supramolecular chemistry strategies have been greatly expanded by the use of metal nanoparticles in combination with molecular species, generating new functional nanostructured materials.[1] The anchoring of molecular species to a metal nanoparticle surface is facilitated by the presence of suitable binding groups, closely paralleling the metal–ligand interaction in coordination chemistry.[2] In this way, coordination compounds containing bridging ligands can be used as the building blocks of three-dimensional networks of interconnected nanoparticles or promote the layer-by-layer assembly of new materials encompassing the cooperative properties of metallic particles and molecular species.

From the supramolecular point of view, trinuclear ruthenium acetate clusters of general formula $[Ru_3O(CH_3COO)_6(L)_3]^+$ (Figure 1) are very useful building blocks of molecular nanomaterials. They exhibit a triangular $[Ru_3O]$ core held together by six acetate bridging ligands with a central oxygen atom behaving as a strongly coupled triruthenium system in addition to three L ligands (solvent, bridging ligands, N-heterocyclic ligands, CO, NO, PPh_3, etc.) at the vertices. Accordingly, they display several monoelectronic redox processes within the –2 to +2 V range, which can be tuned by the peripheral L ligands.[3] Because of their interesting coordination chemistry and electrochemical properties, they have been exploited as carriers of molecular species such as NO[4] and CO,[5] as electron-transfer relays and cofactors of redox catalysts[3c,6] and as active materials in logic gates[7] and electrochromic devices.[8] Bridging ligands such as 4-CNpy, 4,4′-bpy and bpe can be used to bind those complexes to metal or conducting oxide surfaces thereby generating electrochromic, photoelectrochemical and electrochemical interfaces. This may be an interesting approach to the development of new gold-nanoparticle-containing hybrid materials as their properties may be influenced by the molecular species as they can provide tunable binding, redox and electrocatalytic active sites.

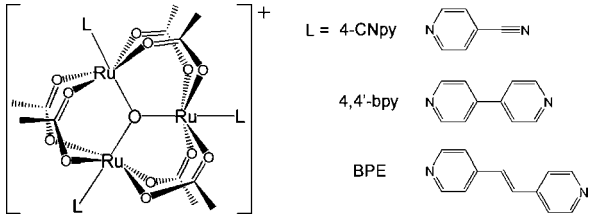

Figure 1. Structural representation of the $[Ru_3O(CH_3COO)_6(L)_3]^+$ cluster complex and of the N-heterocyclic 4-CNpy, 4,4′-bpy and bpe ligands.

Gold nanoparticles (AuNPs) also exhibit interesting electrochemical, catalytic, optical and binding properties[9] that are dependent on their size and plasmon coupling with

[a] Instituto de Química, Universidade de São Paulo,
Av. Prof. Lineu Prestes, 748, CEP 05508-000, Brazil
Fax: +55-11-30913887
E-mail: koiaraki@iq.usp.br

Supporting information for this article is available on the WWW under http://dx.doi.org/10.1002/ejic.201001118.

other nanoparticles as well as the molecular species bound to the surface.[10] In fact, the stabilization, dispersion and functionality of AuNP suspensions are greatly influenced by the hydrophobic/hydrophilic characteristics of the outermost molecular shell. Thus, many synthetic methods have been developed to obtain nanoparticles with labile passivating/stabilizing layers, which are prone to rapid exchange reactions with ligands with higher affinity. Thus, several molecular species exhibiting coordinating groups, such as pyridines, thiols, disulfides and amines,[11] are being used to prepare AuNPs specially designed for application in immunoassays and diagnostics, as well as in molecular electronics, drug delivery and catalysis.[9]

Furthermore, the valence electrons of gold, silver and copper nanoparticles can be excited collectively by electromagnetic radiation giving rise to characteristic surface plasmon bands in the visible region, imparting characteristic red and yellow colours on to the respective dispersions of gold and silver nanoparticles. More interesting, though, is the huge enhancement of the Raman scattering cross-section of molecules adsorbed on their surface [the surface-enhanced Raman scattering (SERS) effect], ascribed to electromagnetic and chemical effects.[12] Accordingly, molecular species already having high Raman scattering cross-sections and suitably tailored binding sites can be used as molecular probes, leading to SERS sensors with much higher sensitivity.[13,14]

In this work, we describe a careful kinetic and spectroscopic study of the interaction between bridging ruthenium cluster complexes and ct-AuNPs, aiming at the preparation of hybrid nanomaterials. This was accomplished by a coordinative layer-by-layer strategy, controlling the deposition of AuNPs and the symmetric triruthenium acetate cluster derivatives with 4-CNpy, 4,4′-bpy and bpe ligands as bridging complexes that exhibit increasing size, as shown in Figure 1.

Results and Discussion

The bridging $[Ru_3O(CH_3COO)_6(L)_3]^+$ complexes can bind to the AuNP surface through one or two sites, leaving at least one free coordination site to bind another nanoparticle. In this way they are suitable bridging complexes for assembling AuNP/$[Ru_3O(CH_3COO)_6(L)_3]^+$ hybrid materials.

The binding strength of these cluster complexes on AuNPs should depend on the nature of the free coordination sites as well as on the hydrophobic/hydrophilic character of the L ligands, which should determine the solvation characteristics and the dispersibility of the resulting nanomaterials. The nitrile group of 4-CNpy is expected to coordinate rather weakly to the AuNP surface, but should exhibit the highest hydrophilic character in the series. On the other hand, the 4,4′-bpy and bpe ligands have similar pyridyl groups, but the latter has an extended π system that should enhance the bonding properties.[3b,3d] In addition, it should impart the highest hydrophobic character to its complex and the corresponding hybrid material.

The evolution of the UV/Vis spectra as a function of time was monitored, particularly at 520 and 700 nm, as shown in parts A–F of Figure 2, to investigate the reaction of $[Ru_3O(CH_3COO)_6(L)_3]Cl$ with ct-AuNPs in aqueous solution. In the case of the bpe and 4,4′-bpy derivatives, rapid and relatively large absorption changes were observed at 700 nm at the beginning of the reaction, which were followed by a more or less steady increase in the absorbance until eventual decrease at much longer times. In fact, the intensities of all the bands decreased with concomitant increase in the baseline absorbance in the last process. In contrast, a sequence of an equal number of processes leading to a decrease in the absorbance was observed at 520 nm (Figure 2, A–D). This behaviour reveals a more or less complex sequence of events involving exchange of citrate ions and surface functionalization followed by association/aggregation of an increasing number of surface-functionalized AuNP units until eventually precipitation takes place (Figure 2, B, D). Note that the kinetic curves at 520 and 700 nm show complementary behaviour, which indicates that both are correlated and reflect the same processes.

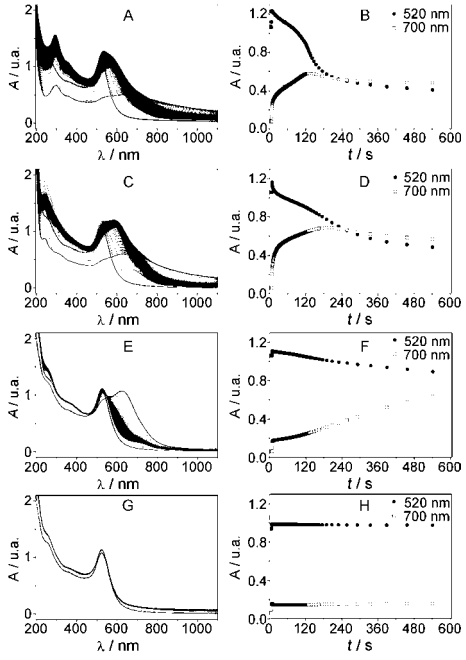

Figure 2. A, B: Evolution of the UV/Vis spectra of ct-AuNP after the addition of $[Ru_3O(CH_3COO)_6(L)_3]^+$ (L = bpe); C, D: L = 4,4′-bpy; E, F: L = 4-CNpy; G, H: L = H_2O. Plots of the absorbance at 520 (●) and 700 nm (□) as a function of time for the respective reactions are shown on the right.

The initial very fast absorption change can be assigned to the mixing process, but it is superimposed by a subsequent fast rise in absorbance at around 600–650 nm without defining a new band. This can be assigned to the bonding of ruthenium complexes and concomitant displacement of citrate ions from the ct-AuNPs surface,[15] a process that changes the solvation properties and the stability of the respective dispersions. Because the L ligands in the ruthenium complexes bonded to the AuNP surface still possess a free coordination site, each of them can bind another nanoparti-

cle, finally generating a three-dimensional coordination network.

The approach of two or more nanoparticles is known to influence the UV/Vis spectrum, decreasing the intensity of the plasmon band at 520 nm and leading to the appearance of a plasmon coupling band, the position and intensity of which are defined by the coupling strength. In fact, as the distance decreases below a certain limit (generally the diameter of the nanoparticles) the coupling strength tends to increase enhancing and shifting that band to the red/near-infrared region.[16] Accordingly, the much slower increase of absorbance at around 700 nm can be assigned to the aggregation of AuNPs functionalized with the ruthenium complexes. This process can proceed interconnecting more and more nanoparticles until reaching a size beyond which precipitation takes place. Precipitation can become the dominant process quite rapidly depending on the hydrophilic/hydrophobic character of the L ligand leading to an exponential decrease of all the absorption bands after around 120 s, as shown in Figure 2 (B, D) for the reactions of $[Ru_3O(CH_3COO)_6(bpe)_3]^+$ and $[Ru_3O(CH_3COO)_6(4,4'\text{-}bpy)_3]^+$ complexes with ct-AuNP.

In contrast, the reaction of $[Ru_3O(CH_3COO)_6(4\text{-}CNpy)_3]^+$ with ct-AuNP exhibited a completely different kinetic behaviour. The absorbance changed very slowly after mixing the reactants and there was no precipitation even after 600 s. However, the absence of precipitate does not mean that the ct-AuNP remained unchanged or that the nanoparticles do not aggregate. In fact, the reaction led to the appearance of a strong and well-defined plasmon coupling band at 640 nm (Figure 2, E), confirming the presence of aggregates in solution. However, they seem to grow much more slowly, probably because of the higher solubility, lower affinity and higher lability of the nitrile–AuNP bonds that should also limit the size of the aggregates.

Furthermore, the AuNPs should be much closer to each other than in the aggregates formed by the $[Ru_3O(CH_3COO)_6(bpe)_3]^+$ and $[Ru_3O(CH_3COO)_6(4,4'\text{-}bpy)_3]^+$ complexes because 4-CNpy is the smallest of the three bridging ligands. On the other hand, bpe is the largest and should keep the nanoparticles separated by larger distances in the corresponding hybrid material. This reflects directly on the plasmon coupling strength and on the position of the respective absorption bands.[17] Accordingly, the more intense and red-shifted plasmon coupling band observed for aggregates of AuNPs bridged by $[Ru_3O(CH_3COO)_6(4\text{-}CNpy)_3]^+$, as compared with those bridged by $[Ru_3O(CH_3COO)_6(bpe)_3]^+$ (Figure 2, A, C), can be easily explained by their size. The aggregates of the AuNPs bridged by the $[Ru_3O(CH_3COO)_6(4,4'\text{-}bpy)_3]^+$ complex exhibited an intermediary behaviour (Figure 2, E) reinforcing the validity of our hypothesis (see the Supporting Information).

The influence of electrostatic effects on the aggregation process was probed by using the triruthenium aqua complex $[Ru_3O(CH_3COO)_6(H_2O)_3]^+$, which has no coordination site available for binding on the AuNP surface. In fact, no change was observed in the UV/Vis spectrum or in the kinetic profile until up to 600 s (Figure 2, G, H), which shows that there is no significant electrostatic contribution to the aggregation process. The presence of $[Ru_3O(CH_3COO)_6(H_2O)_3]^+$ complexes in solution is confirmed by a characteristic weak intracluster transition (IC) band at 700 nm.

SPR Spectroscopic Investigation of the Layer-by-Layer Assembly

One can expect that the spectroscopic and, in particular, electrochemical properties of the $[Ru_3O(CH_3COO)_6(L)_3]^+$ complexes will impart new conduction and/or electrocatalytic properties on to the hybrid materials. However, it is more convenient to generate them in a controlled way, for instance, on an electrode surface to access their electrochemical properties. Among the methods that can be used for such a purpose, the layer-by-layer method is a very interesting one because it allows control of the composition and thickness. Electrostatic interactions of molecular species and polymeric electrolytes are commonly used as the driving force, but there are a few examples using a cationic and anionic molecular species.[3c,18] Another possibility is the use of metal–ligand coordination bonds to assemble thin films, as demonstrated by monitoring spectrophotometrically the successive deposition reactions of ditopic terpyridine derivatives and transition-metal ions.[19] This coordinative assembly method was adopted in our experiments, but the in situ synthesis of a hybrid material on the top of a substrate depends on factors such as reaction kinetics, solubility and lability/inertness of the bonds involved in the construction process. To understand these factors, a careful study was carried out by using surface plasmon resonance (SPR) spectroscopy.

Organothiol monolayers are generally formed in two steps, as previously shown by SPM, ellipsometry and contact angle measurements.[20] The first step is fast and takes place in a few minutes over 60–90% of the surface area and is influenced by factors such as the organothiol concentration, the alkyl group, the position of the thiol group in the chain, the temperature, the solvent and the surface characteristics of the substrate, as demonstrated by Damos et al.[21] using mercaptoundecanoic acid. First, a sub-monolayer coverage is obtained in which the alkyl chains are more or less randomly oriented. This is followed by their rearrangement assuming an angle between 27–48° relative to the normal,[22,23] which generates a more compact and organized monolayer.

The adsorption of any species onto SPR substrates influences the electron density and/or the mass of the thin gold layer thus changing the surface plasmon resonance angle. Interestingly, the quite large random fluctuations observed for the bare substrates disappeared after functionalization of the gold surface with a compact monolayer of 1,4-butanedithiol (24 h, methanol solution). After SAM formation, the SPR signal can be assigned to molecular interactions with the alkanethiol groups on the surface, which lead to its stabilization and consequent enhancement of the sig-

nal-to-noise ratio. These surface-modified SPR substrates were then used in experiments aimed at studying the deposition processes that lead to AuNP/$[Ru_3O(CH_3COO)_6(L)_3]^+$ hybrids. Accordingly, they were placed in the cell and exposed to ct-AuNP solution, washed with deionized water, treated with a ruthenium complex solution and washed again with deionized water to remove the excess of the complex, as shown in Figure 3. These steps were repeated in each of the subsequent cycles in the construction process.

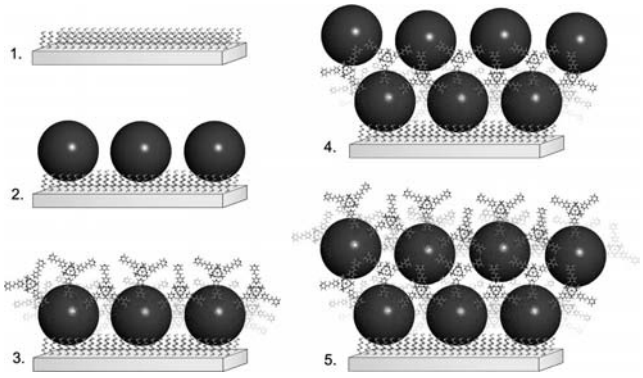

Figure 3. Scheme showing the modification of a gold substrate with a compact monolayer of 1,4-butanedithiol (**1**) and subsequent construction of AuNP/$[Ru_3O(CH_3COO)_6(L)_3]^+$ hybrid materials by layer-by-layer coordinative assembly that encompasses the binding of ct-AuNP (**2**) and of the $[Ru_3O(CH_3COO)_6(bpe)_3]^+$ complex (**3**), and repetition of the last two steps to give a second monolayer (**4** and **5**).

The respective kinetic curves, that is, the changes in SPR angle ($\Delta\theta$) as a function of time, are shown in Figure 4 (A, C, E) and the intensity of the laser beam reflection as a function of SPR angle after successive injection steps are shown in Figure 4 (B, D, F). The injection of the ct-AuNP dispersion led to an exponential increase in $\Delta\theta$ until reaching saturation, as expected for the interaction of ct-AuNPs forming a reasonably densely packed monolayer on the surface. The subsequent injection of the $[Ru_3O(CH_3COO)_6(L)_3]^+$ complex solution leads to a fast increase in $\Delta\theta$, which can be divided into two contributions. Immediately after the injection there is an instantaneous increase in $\Delta\theta$, probably as a result of the electrostatic interaction of the negatively charged ct-AuNP layer with the positively charged triruthenium clusters in addition to changes in the ionic strength and refractive index. This is followed by an exponential increase in $\Delta\theta$ consistent with the coordination of the triruthenium cluster complexes to the AuNP surface, which generates a monolayer of AuNP/$[Ru_3O(CH_3COO)_6(L)_3]^+$ material. However, the contribution of this second component is much smaller for $[Ru_3O(CH_3COO)_6(4\text{-}CNpy)_3]^+$ than for the corresponding bpe and 4,4′-bpy derivatives, which confirms the lower affinity of the 4-CNpy complex for the AuNP surface.

Interestingly, up to five times larger changes in $\Delta\theta$ were observed when the second layer of ct-AuNP was deposited, which suggests that much larger amounts of gold nanoparticles were bonded to the surface. This is further confirmed by the proportionally larger change in $\Delta\theta$ in the subsequent

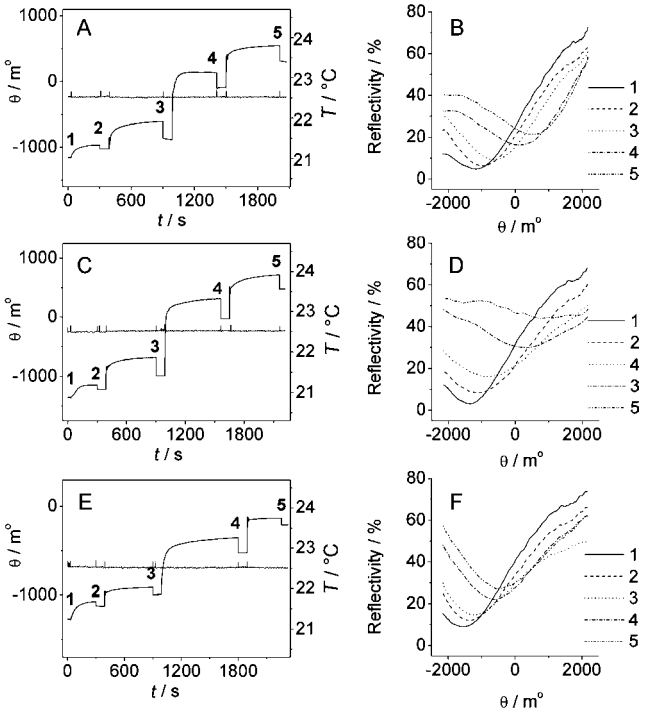

Figure 4. SPR curves of $\Delta\theta$ vs. time and the intensity of the laser beam reflection as a function of the SPR angle during successive reactions of 1,4-butanedithiol-functionalized substrates with ct-AuNP and $[Ru_3O(CH_3COO)_6(L)_3]^+$ complexes (A, B: L = bpe, C, D: 4,4′-bpy, E, F: 4-CNpy). i. Injection of the ct-AuNP suspension; ii. washing step followed by treatment with the cluster solution; iii. washing step and successive injection of the ct-AuNP dispersion; iv. subsequent washing and injection of triruthenium cluster solution; v. washing with deionized water.

coordination of $[Ru_3O(CH_3COO)_6(L)_3]^+$ complexes. The excess reagent was rinsed with deionized water before injection of the next reagent leading to an instantaneous decrease in the SPR signal. Nevertheless, there was always an overall increase in the SPR baseline signal, which confirms the bonding of the reagents to the surface. In fact, the kinetic curves can be easily analysed, particularly by comparison of the $\Delta\theta$ and slopes. Thus, the binding rates seem to follow the same trend observed for the citrate substitution kinetics on ct-AuNP in aqueous solution, that is, bpe > 4,4′-bpy >> 4-CNpy.

Raman and SERS Spectroscopy

Raman and SERS spectroscopy are interesting techniques for investigating the binding of molecular species to gold nanoparticles. Accordingly, a thorough study was carried out by using the pure $[Ru_3O(CH_3COO)_6(bpe)_3]^+$, $[Ru_3O(CH_3COO)_6(4,4'\text{-}bpy)_3]^+$ and $[Ru_3O(CH_3COO)_6(4\text{-}CNpy)_3]^+$ complexes as well as the corresponding hybrid nanomaterials. Films of AuNP/$[Ru_3O(CH_3COO)_6(L)_3]^+$ were prepared by the layer-by-layer assembly method and studied by Raman and SERS spectroscopy using 785 and 532 nm excitation laser lines.

The bpe ligand has one of the highest Raman scattering cross-sections, according to Zhuang et al.,[24] exhibiting two

coordinating pyridyl sites at opposite symmetric positions of a delocalized π system, which makes them almost ideal as molecular probes for SERS purposes. It is formed of 24 atoms and exhibits 33 normal ($23A_g + 10B_g$) and 33 fundamental ($11A_u + 22B_u$) vibrational modes in the *trans* conformation (C_{2h} symmetry). Half of them are Raman-active and assigned to in-plane (ip) A_g and B_u, and out-of-plane (op) A_u and B_g vibrational modes. Furthermore, some IR-active A_u and B_u fundamental modes can also be observed in the Raman[25] spectra of the free and bonded bpe ligand, as shown in Figure 5A. The tentative assignments for the pure complex and the complex in the hybrid material were made by comparison with the vibrational modes of the free bpe ligand and the triruthenium acetate complexes found in the literature,[26] as shown in Table S1 in the Supporting Information.

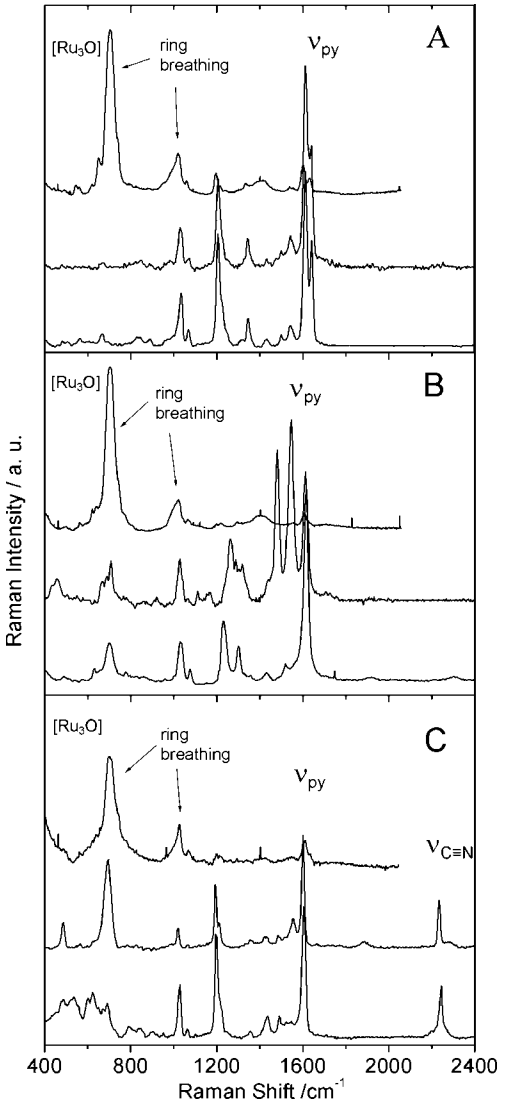

Figure 5. FT Raman spectra of solid $[Ru_3O(CH_3COO)_6(L)_3]PF_6$ complexes (bottom) and AuNP/$[Ru_3O(CH_3COO)_6(L)_3]^+$ films (middle) at λ_{exc} = 532 nm and 785 nm (top) for A: bpe, B: 4,4′-bpy and C: 4-CNpy cluster derivatives.

When molecules are covalently bonded to a metal surface, changes in the energies of the vibrational modes are expected. In fact, the band at 995 cm^{-1}, assigned to the breathing mode of the pyridyl ring of the non-coordinated bpe ligand, was found to be shifted to 1011 cm^{-1} when bonded to a metallic silver surface[24] and to 1033 cm^{-1} when coordinated to the triruthenium cluster complex (see Table S1 in the Supporting Information). In contrast, physisorbed molecules generally show much smaller shifts and band-broadening.[27] However, the changes observed in the Raman spectra shown in Figure 5 as a function of the excitation wavelength cannot be assigned only to these effects. In fact, the amount of triruthenium cluster per volume is much smaller in the hybrid material than in the pure complex.

The spectra of solid $[Ru_3O(CH_3COO)_6(bpe)_3]PF_6$ and AuNP/$[Ru_3O(CH_3COO)_6(bpe)_3]^+$ are similar when excited at 532 nm, as can be seen in part A of Figure 5, and typical bpe vibrational bands can be found at around 900 and 1700 cm^{-1}. However, the Raman spectrum of the hybrid material at λ_{exc} = 785 nm is remarkably different, exhibiting medium intensity and broad peaks at around 1000 and 1400 cm^{-1} as well as an intense peak at 650 cm^{-1}, which is absent in the spectra at λ_{exc} = 532 nm. Unfortunately, it was not possible to record the Raman spectra of the pure cluster complexes because decomposition takes place when irradiated with the 785 nm laser, probably as a consequence of the resonance with the broad intracluster (IC) band at 700 nm. Thus, the intensification of the cluster vibrational modes observed for the AuNP/$[Ru_3O(CH_3COO)_6(bpe)_3]^+$ hybrid at λ_{exc} = 785 nm can be accounted for by the resonance Raman (rR) effect. This may be responsible for the enhancements of up to six orders of magnitude in the Raman scattering cross-section of selected vibrational modes of the chromophore.

The $[Ru_3O]$ core has four Raman-active vibrational modes (ν_{as}, ν_s, δ_{as} and δ_s) below 750 cm^{-1}.[28] The bands at 708 and 543 cm^{-1} (respectively assigned to ν_{as} and δ_s), both absent at λ_{exc} = 532 nm, were observed in the spectrum of the complex at λ_{exc} = 785 nm, thereby providing evidence for a large contribution from the rR effect associated with the IC band at 700 nm. Also, there is some contribution of chemical effects ascribed to charge-transfer interactions between the nanoparticles and the adsorbed molecules, changing its polarizability.

However, enhancements of up to 15 orders of magnitude have been reported[12] for molecules adsorbed on gold or silver nanoparticles, which cannot be accounted for by only considering the resonance and chemical effects. In fact, the enhancement of the local electric field of nanomaterials by coupling of the surface plasmon fields with the oscillating electric field of light was shown to be responsible for very high intensification effects. This is observed at special points on a nanostructured surface or at the junction between nanoparticles called hot spots, which play a major role in the SERS effect. Thus, the strong intensification of the breathing modes of the pyridine ring and vibrational modes of the acetate bridge of the $[Ru_3O]$ centre at around 670 cm^{-1} are consistent with both the rR and SERS effects and can be assigned to a surface-enhanced resonance Ra-

man scattering (SERRS) effect. The Raman spectral behaviour of the other two derivatives can be explained similarly, as discussed below.

The Raman spectrum of the pure 4,4′-bpy ligand exhibits characteristic bands at 659, 755, 997, 1219, 1293, 1508 and 1607 cm^{-1}. Some of these bands can be influenced by coordination to the $[Ru_3O]$ core and AuNP surface, depending on the bond conformation and geometry. In fact, the changes in the Raman spectra of pyridine, bipyridine and analogous ligands bonded to metal surfaces were used to study the adsorption geometry of these molecules, giving relevant information about their bonding properties.

The FT Raman spectra of the solid $[Ru_3O(CH_3COO)_6(4,4'\text{-bpy})_3]PF_6$ complex and AuNP/$[Ru_3O(CH_3COO)_6(4,4'\text{-bpy})_3]^+$ hybrid are shown in Figure 5 (B). The tentative assignment shown in Table S2 in the Supporting Information was carried out by comparison with the spectra of the 4,4′-bpy ligand and analogous triruthenum cluster derivatives found in the literature,[26] as discussed above.

Note that the spectra of the hybrid material and the corresponding triruthenium cluster complex at λ_{exc} = 532 nm are similar, except for the rise of two strong peaks at 1424 and 1544 cm^{-1}, which suggests that there are significantly different bonding effects induced by the coordination of the $[Ru_3O(CH_3COO)_6(4,4'\text{-bpy})_3]^+$ complex to AuNPs. Indeed, the 4,4′-bpy ligand has been proven to bond perpendicularly to the Au(111)[29] surface, acting as a metallic junction between two electrodes.[30,31] Such behaviour is interesting because bpe also has a pair of pyridyl groups but connected by an ethylene bridge, which can also allow significant electronic coupling when in an *all-trans* conformation. What is remarkable though is the similarity of the Raman spectra of the AuNP hybrids with the bpe and 4,4′-bpy cluster derivatives at λ_{exc} = 785 nm. This behaviour is consistent with simultaneous rR and SERS intensification effects arising from the interactions of the 4,4′-bpy and bpe ligands with both AuNPs and the $[Ru_3O]$ core.

4-CNpy is also known to be a good bridging ligand, particularly for Pt, Au and Ag nanoparticles, because of the nitrile group located at the *para* position relative to the pyridyl N atom.[32] This ligand can change the adsorption geometry on gold surfaces depending on the applied electrochemical potential.[33] In fact, it has been shown to adsorb i. vertically through a pyridyl N atom σ bond at negative potentials, ii. assume a planar conformation by means of π interactions or iii. adsorb through a nitrile N atom σ bond at positive potentials.[34]

The SERS spectra of the solid $[Ru_3O(CH_3COO)_6(4\text{-CNpy})_3](PF_6)$ complex and AuNP/$[Ru_3O(CH_3COO)_6(4\text{-CNpy})_3]^+$ hybrid nanomaterial are shown in Figure 5 (C) and the tentative assignment is listed in Table S3 in the Supporting Information. The free ligand exhibits intense peaks at 1601, 1194 and 997 cm^{-1}, assigned to pyridine ring vibrational modes.[35] These modes, particularly the ring breathing mode at 997 cm^{-1}, are strongly influenced by coordination to the metal surface through the pyridyl N atom. In fact, the peaks at 1601, 1194 and 997 cm^{-1} were shifted, respectively, to 1605, 1193 and 1017 cm^{-1} when bonded to the gold surface.[34] Similar behaviour was observed for the $[Ru_3O(CH_3COO)_6(4\text{-CNpy})_3]PF_6$ complex, which confirms its preferential coordination through the pyridyl N atom. Nevertheless, major shifts were observed for the vibrational modes involving the CN group in the AuNP/$[Ru_3O(CH_3COO)_6(4\text{-CNpy})_3]^+$ hybrid material, as expected for the coordination of the complex to AuNPs through the N atom. In fact, the in-plane and out-of-plane angular deformation modes at 771, 638 and 490 cm^{-1} are the most strongly affected, as can be seen in Table S3 in the Supporting Information. All these peaks are shifted to a lower energy relative to the corresponding free ligand modes, which reflects the decrease in the bond strength as a consequence of back-bonding interactions. Unfortunately, photodegradation precluded the study of the Raman spectra of pure $[Ru_3O(CH_3COO)_6(L)_3]PF_6$ complexes at λ_{exc} = 785 nm.

Electrocatalytic Properties of the Hybrid Material

Fluorine-doped tin oxide (FTO) electrodes modified with thin films of AuNP/$[Ru_3O(CH_3COO)_6(L)_3]^+$ were prepared to evaluate their electrocatalytic properties towards the oxidation of nitrite to nitrate. The electrode surface was first modified with 3-(mercaptopropyl)trimethoxisilane (MPTS) before starting to construct the hybrid nanomaterial by the coordinative layer-by-layer assembly method. All samples were prepared by repeating three times the deposition of ct-AuNP and the $[Ru_3O(CH_3COO)_6(\mathbf{L})_3](PF_6)$ complex using a procedure similar to that described above in the SPR experiments. The corresponding SEM images are shown in Figure 6.

Reasonably compact films were obtained for AuNP/$[Ru_3O(CH_3COO)_6(bpe)_3]^+$, whereas AuNP/$[Ru_3O(CH_3COO)_6(4,4'\text{-bpy})_3]^+$ was more sparsely distributed but still with a good coverage. As expected, much lower coverages were obtained for the AuNP/$[Ru_3O(CH_3COO)_6(4\text{-CNpy})_3]^+$ hybrid. All experiments were performed at least in triplicate giving reproducible results, which clearly reflect the influence of the AuNP–cluster complex bond stability/lability and solubility on the film construction process. The strong influence of the cluster L ligands correlates well with the tendency for coordinatively induced aggregation and the precipitation/deposition process observed in solution and on the gold surface, that is, bpe > 4,4′-bpy >> 4-CNpy. Thus, the electrochemical experiments were carried out only with the first two derivatives.

Gold itself is known to catalyse the electrochemical oxidation of nitrite to nitrate in aqueous solution at potentials of around 1 V.[36] Similar electrocatalytic activity but much higher sensitivity were observed for the AuNP/$[Ru_3O(CH_3COO)_6(bpe)_3]^+$- and AuNP/$[Ru_3O(CH_3COO)_6(4,4'\text{bpy})_3]^+$-modified FTO electrodes.

The onset and the peak of the electrocatalytic wave of the latter modified electrode were found to be 0.82 and 1.0 V, whereas the bpe derivative exhibited these peaks at 0.76 and 0.95 V, respectively. The sensitivity of this electrode (12.8×10^{-2} μA μM^{-1}) was much higher than that of

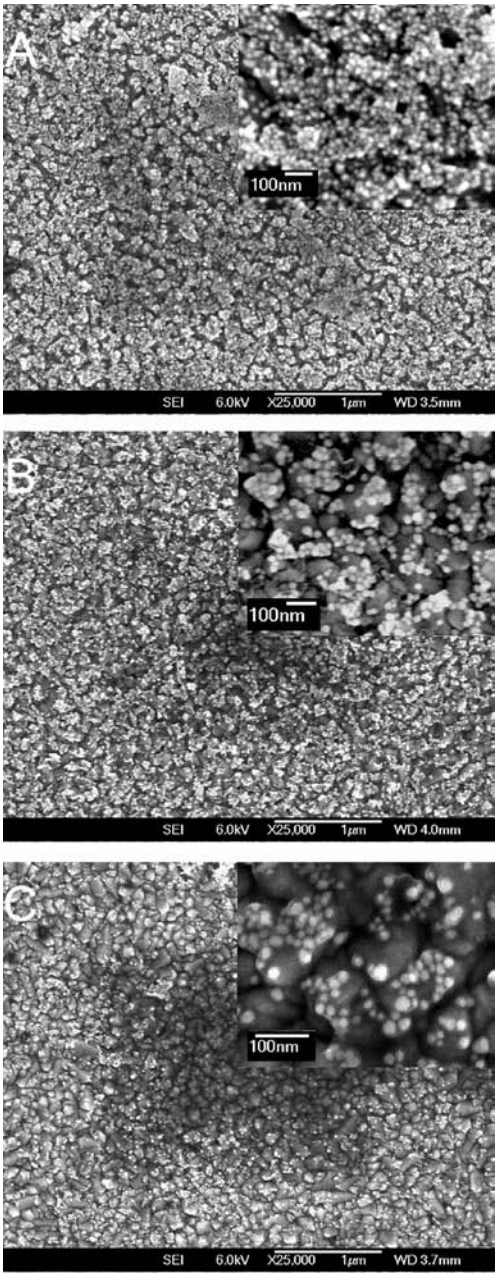

Figure 6. SEM images of FTO electrodes modified with 3-(mercaptopropyl)trimethoxisilane and subsequently submitted to three deposition cycles of AuNP/$[Ru_3O(CH_3COO)_6(L)_3]^+$ hybrid materials. A: bpe, B: 4,4′-bpy, C: 4-CNpy. Inset: magnification showing the integrity of the AuNPs and their density on the films.

the 4,4′-bpy derivative (9.25×10^{-2} μA μM^{-1}). This can be explained by the relative surface coverages of the corresponding hybrid materials, but the cathodic shifts of the electrocatalytic peaks suggest a significant influence of the triruthenium complex on the electrocatalytic properties. Furthermore, the modified electrodes exhibited enhanced sensitivity compared with conventional bare gold electrodes, probably as a consequence of the much higher surface area. In fact, an excellent linear correlation for the current versus $[NO_2^-]$ plot was obtained (R = 0.9995) in the $[NO_2^-]$ range of 0.5–1000 μmol L^{-1}, as shown in Figure 7.

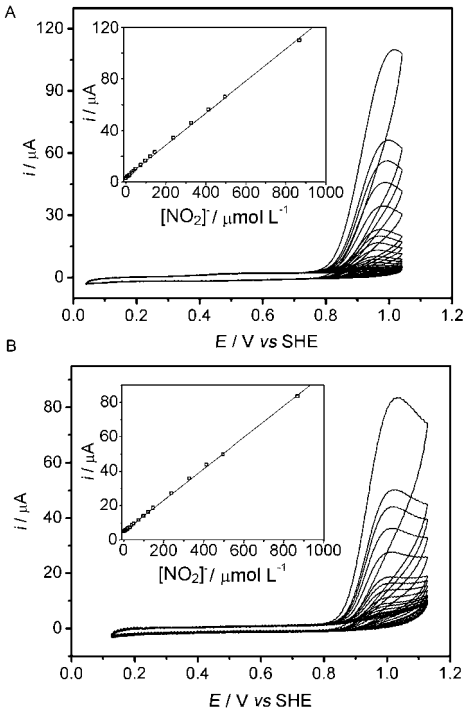

Figure 7. Cyclic voltammograms of FTO electrodes modified with A) AuNP/$[Ru_3O(CH_3COO)_6(bpe)_3]^+$ and B) AuNP/$[Ru_3O(CH_3COO)_6(4,4'\text{-bpy})_3]^+$ upon addition of increasing concentrations of $NaNO_2$ in 0.1 M KNO_3 electrolyte solution (v = 100 mV s^{-1}). Inset: plot of peak current vs. $[NO_2^-]$.

Conclusions

The $[Ru_3O(CH_3COO)_6(L)_3]PF_6$ complexes rapidly bind to ct-AuNPs leading to surface functionalization and subsequent aggregation due to the formation of interparticle bonds, reflecting the characteristics of the L bridging ligand and the bond strength sequence bpe > 4,4′-bpy >> 4-CNpy. The preferential binding of the L bridging ligands to the $[Ru_3O]$ core through the pyridyl N atom was also confirmed by Raman spectroscopy as well as SERS and SERRS effects. The SEM images of FTO electrodes modified with AuNP/$[Ru_3O(CH_3COO)_6(L)_3]$ by coordinative layer-by-layer assembly are consistent with the kinetic and SPR data, showing the formation of sufficiently compact thin films with the bpe and 4,4′-bpy triruthenium cluster derivatives, which indicates that the stability/lability of AuNP–cluster bonds as well the solubility are important parameters influencing the film construction process. The enhanced sensitivity and the electrocatalytic response of the AuNP/$[Ru_3O(CH_3COO)_6(L)_3]^+$ hybrid materials have been shown to depend on the bridging complex in the oxidation of nitrite to nitrate, which demonstrates their high potential for application in amperometric sensors.

Experimental Section

Materials: The $[Ru_3O(CH_3COO)_6(4\text{-CNpy})_3]PF_6$, $[Ru_3O(CH_3COO)_6(4,4'\text{-bpy})_3]PF_6$ and $[Ru_3O(CH_3COO)_6(bpe)_3]PF_6$ clusters were prepared according to an adaptation of previously described

procedures for related species.[3b,5a,37] Briefly, a methanol solution of the $[Ru_3O(CH_3COO)_6(CH_3OH)_3](CH_3COO)$ complex was added dropwise to at least a three-fold excess of 4-CNpy, 4,4′-bpy and bpe in methanol solution and the mixture was heated at reflux for 30 min. The dark precipitate was filtered, washed with small volumes of cold water and methanol, and dried in a desiccator under vacuum. Then a stoichiometric amount of Br_2, diluted in CH_2Cl_2, was slowly added to a magnetically stirred suspension of the $[Ru_3O(CH_3COO)_6(L)_3]$ complex in CH_2Cl_2 (50 mL). Finally, the solvent was removed in a rotary evaporator and the solid was redissolved in methanol and precipitated by addition of an aqueous solution of NH_4PF_6 (ca. five-fold excess). The mixture was kept in the refrigerator for 48 h, the dark-green precipitate was filtered off, washed with cold methanol and diethyl ether and dried in a dessicator under vacuum. The final purification was carried out by neutral alumina column chromatography (20×1.5 cm) using a 1:1 v/v mixture of ethyl acetate/acetonitrile as eluent. The solvent was removed in a flash evaporator and dried under vacuum.

$[Ru_3O(CH_3COO)_6(4\text{-}CNpy)_3]PF_6$: Yield ca. 50%. $C_{30}H_{30}F_6N_6O_{13}PRu_3$ (1130.9): calcd. C 31.87, H 2.67, N 7.43; found C 31.70, H 2.94, N 7.15. MS (ESI): one peak at m/z = 987.0; $\Delta(m/z)$ = 1.0 corresponding to the molecular ion.

$[Ru_3O(CH_3COO)_6(4,4'\text{-}bpy)_3]PF_6$: Yield ca. 35%. $C_{42}H_{42}F_6N_6O_{13}PRu_3$ (1287.0): calcd. C 39.20, H 3.29, N 6.53; found C 39.10, H 3.89, N 6.40. MS (ESI): one peak at m/z = 1142.9; $\Delta(m/z)$ = 1.0 corresponding to the molecular ion.

$[Ru_3O(CH_3COO)_6(bpe)_3]PF_6$: Yield ca. 25%. $C_{48}H_{48}F_6N_6O_{13}PRu_3$ (1365.10): calcd. C 42.23, H 3.54, N 6.16; found C 41.92, H 3.92, N 6.03. MS (ESI): one peak at m/z = 1221.1; $\Delta(m/z)$ = 1.0 corresponding to the molecular ion.

ct-AuNP: Stable suspensions in water were prepared by using the method of Turkevich et al.[38] Typically, an aqueous $HAuCl_4 \cdot 3H_2O$ (Aldrich) solution (0.03% *m*/*v*, 100 mL) was heated up to the boiling temperature and then a sodium citrate solution (1% *m*/*v*, 2.75 mL) was added all at once under vigorous stirring. The reaction mixture immediately turned dark blue, then bluish red and finally bright red. This colour is characteristic of ct-AuNPs of 20–30 nm diameter, stabilized by citrate ions bound to the surface. However, they are labile and can be readily exchanged by molecules exhibiting suitable coordinating groups.

Physical Measurements: A suspension of ct-AuNP was diluted to adjust the absorbance of the plasmon band at 520 nm to 1 u.a. (ca. 2.0×10^{-4} mol L^{-1} of gold atoms in ca. 20 nm nanoparticles or ca. 2×10^{-5} mol L^{-1} of surface gold atoms) and treated with a 3×10^{-3} mol L^{-1} $[Ru_3O(CH_3COO)_6(L)_3]Cl$ aqueous solution. The chloride salts were obtained by exchanging the counterion PF_6^- for Cl^-, adding the PF_6^- salt solution to a saturated LiCl solution in acetone, collecting and drying the precipitate. The reaction was carried out inside a 10.0 mm quartz cuvette containing ct-AuNPs suspension (3.0 mL) and by adding the corresponding ruthenium complex solution (30 μL) whilst stirring. The evolution of the reaction was monitored spectrophotometrically at 1 s intervals by using a HP-8453A diode array spectrophotometer in the kinetic mode.

Raman spectra in the 350–2000 cm^{-1} range were obtained by using an InPhotonics spectrophotometer equipped with a 785 nm laser (P_{max} = 250 mW cm^{-2}) and a bundled fibre optics probe. All measurements were carried out by using a sample-to-probe distance of 2 mm, an integration time of 120 s and 70% of the maximum laser power. The Raman scattering spectra, exciting with a 532 nm argon laser (P_{max} = 100 mW), were recorded with a WITec Alpha 300R Raman confocal microscope, an integration time of 120 s, 20X objective and a numeric aperture of 0.4 in the 100–3200 cm^{-1} spectral range.

The SPR spectra were recorded with an EcoChemie AutoLab SPRINGLE instrument using the Kretschmann arrangement and a diode laser (λ = 680 nm). The special glass substrate covered with a 50 nm thick gold layer was cleaned with piranha solution for 15 min, washed with deionized water and kept in a 1×10^{-4} mol L^{-1} aqueous solution of 1,4-butanedithiol for 24 h. Then it was mounted in the SPR cell and exposed successively to solutions of ct-AuNP and triruthenium cluster complexes (1×10^{-4} mol L^{-1}), intercalated by rinsing steps with deionized water. All processes were carried out continuously and automatically using 50 μL samples and a flux of 10 μL s^{-1}. The cell was kept at 25 °C by using a Pharmacia LKB multi-temp II thermostatted bath.

The FTO substrates ($A = 1.0 \times 1.5$ cm^2) were cleaned by dipping them into a piranha solution activated with a $H_2O/H_2O_2/NH_4OH$ (5:1:1 v/v) mixture for 15 min and then treating them with a 1.0×10^{-3} mol L^{-1} solution of 3-(mercaptopropyl)trimethoxysilane (3MPTS) in methanol for 6 h. Thin films of the hybrid materials were constructed on top of 3-MPTS modified substrates by coordinative assembly, dipping them successively into an aqueous ct-AuNP solution and then into a methanolic triruthenium cluster solution for 10 min. After each deposition step the electrodes were carefully washed with the corresponding solvent to remove the excess of reactant and assure the formation of AuNP/triruthenium cluster hybrid materials for the spectroscopic, electrochemical and morphological characterization.

The electrochemical measurements were carried out in a 0.1 mol L^{-1} KNO_3 solution containing 1.0×10^{-2} mol L^{-1} acetate buffer (pH = 4.7) as electrolyte. The 1.0×10^{-3} mol L^{-1} $NaNO_2$ solution was prepared by using the same electrolyte solution. The cyclic voltammograms (CV) were recorded by using an AutoLab PGSTAT30 potentiostat/galvanostat and a conventional three-electrode cell arrangement with an Ag/AgCl (1.0 mol L^{-1} KCl) reference electrode, a coiled platinum wire counter-electrode and a modified FTO substrate as the working electrode. The SEM images were obtained with a JEOL JSM-7401 scanning electron microscope using a typical acceleration voltage of 6 KeV.

Supporting Information (see footnote on the first page of this article): Tentative assignment of the FT-Raman spectra (Tables S1–S3) of pure $[Ru_3O(CH_3COO)_6(L)_3]PF_6$, AuNP/$[Ru_3O(CH_3COO)_6(L)_3]$ hybrid material and the free L ligand; UV/Vis spectra (Figure S1) of ct-AuNPs aqueous solution and AuNP/$[Ru_3O(CH_3COO)_6(L)_3]$ hybrids showing the deconvolution of the plasmon coupling band; and TEM images (Figure S2) of ct-AuNP and AuNP/$[Ru_3O(CH_3COO)_6(BPE)_3]^+$ hybrid material on cooper grid.

Acknowledgments

The authors thank the financial support of Fundação de Amparo a Pesquisa do Estado de São Paulo (FAPESP), Conselho Nacional de Desenvolvimento Científico e Tecnológico (CNPq) and Petróleo Brasileiro (Petrobrás).

[1] a) A. B. Descalzo, R. Martinez-Manez, R. Sancenon, K. Hoffmann, K. Rurack, *Angew. Chem.* **2006**, *118*, 6068; *Angew. Chem. Int. Ed.* **2006**, *45*, 5924–5948; b) M. Meilikhov, K. Yusenko, D. Esken, S. Turner, G. Van Tendeloo, R. A. Fischer, *Eur. J. Inorg. Chem.* **2010**, 3701–3714.

[2] H. E. Toma, V. M. Zamarion, S. H. Toma, K. Araki, *J. Braz. Chem. Soc.* **2010**, *21*, 19.

[3] a) M. Abe, T. Michi, A. Sato, T. Kondo, W. Zhou, S. Ye, K. Uosaki, Y. Sasaki, *Angew. Chem.* **2003**, *115*, 3018; *Angew. Chem. Int. Ed.* **2003**, *42*, 2912–2915; b) H. E. Toma, C. J. Da Chunha, C. Cipriano, *Inorg. Chim. Acta* **1988**, *154*, 63–66; c) H. E. Toma, K. Araki, *Prog. Inorg. Chem.* **2009**, *56*, 379–485; d) S. H. Toma, A. D. P. Alexiou, H. E. Toma, K. Araki, M. N. Eberlin, *J. Mass Spectrom.* **2009**, *44*, 361–367; T. Michi, M. Abe, S. Takakusagi, M. Kato, K. Uosaki, Y. Sasaki, *Chem. Lett.* **2008**, *37*, 576–577.

[4] a) H. E. Toma, A. D. P. Alexiou, A. L. B. Formiga, M. Nakamura, S. Dovidauskas, M. N. Eberlin, D. M. Tomazela, *Inorg. Chim. Acta* **2005**, *358*, 2891–2899; b) H. E. Toma, A. D. P. Alexiou, S. Dovidauskas, *Eur. J. Inorg. Chem.* **2002**, 3010–3017; c) S. Ye, W. Zhou, M. Abe, T. Nishida, L. F. Cui, K. Uosaki, M. Osawa, Y. Sasaki, *J. Am. Chem. Soc.* **2004**, *126*, 7434–7435; d) W. Zhou, Y. Zhang, M. Abe, K. Uosaki, M. Osawa, Y. Sasaki, S. Ye, *Langmuir* **2008**, *24*, 8027–8035; e) S. D. Glover, J. C. Goeltz, B. J. Lear, C. P. Kubiak, *Coord. Chem. Rev.* **2010**, *254*, 331–345.

[5] a) J. A. Baumann, D. J. Salmon, S. T. Wilson, T. J. Meyer, W. E. Hatfield, *Inorg. Chem.* **1978**, *17*, 3342–3350; b) S. Ye, H. Akutagawa, K. Uosaki, Y. Sasaki, *Inorg. Chem.* **1995**, *34*, 4527–4528; c) M. Abe, T. Masuda, T. Kondo, K. Uosaki, Y. Sasaki, *Angew. Chem.* **2005**, *117*, 420; *Angew. Chem. Int. Ed.* **2005**, *44*, 416–419; d) W. Zhou, S. Ye, M. Abe, T. Nishida, K. Uosaki, M. Osawa, Y. Sasaki, *Chem. Eur. J.* **2005**, *11*, 5040–5054.

[6] a) H. E. Toma, K. Araki, A. D. P. Alexiou, S. Nikolaou, S. Dovidauskas, *Coord. Chem. Rev.* **2001**, *219*, 187–234; b) G. S. Nunes, A. D. P. Alexiou, K. Araki, A. L. B. Formiga, R. C. Rocha, H. E. Toma, *Eur. J. Inorg. Chem.* **2006**, 1487–1495.

[7] L. F. O. Furtado, A. D. P. Alexiou, L. Goncalves, H. E. Toma, K. Araki, *Angew. Chem.* **2006**, *118*, 3215; *Angew. Chem. Int. Ed.* **2006**, *45*, 3143–3146.

[8] a) S. H. Toma, H. E. Toma, *Electrochem. Commun.* **2006**, *8*, 1628–1632; b) M. Itou, Y. Araki, O. Ito, H. Kido, *Inorg. Chem.* **2006**, *45*, 6114–6116.

[9] M. C. Daniel, D. Astruc, *Chem. Rev.* **2004**, *104*, 293–346.

[10] G. Schmid, B. Corain, *Eur. J. Inorg. Chem.* **2003**, 3081–3098.

[11] a) S. H. Toma, J. A. Bonacin, K. Araki, H. E. Toma, *Eur. J. Inorg. Chem.* **2007**, 3356–3364; b) F. S. Nunes, L. D. Bonifacio, K. Araki, H. E. Toma, *Inorg. Chem.* **2006**, *45*, 94–101.

[12] J. R. Lombardi, R. L. Birke, *Acc. Chem. Res.* **2009**, *42*, 734–742.

[13] S. W. Bishnoi, C. J. Rozell, C. S. Levin, M. K. Gheith, B. R. Johnson, D. H. Johnson, N. J. Halas, *Nano Lett.* **2006**, *6*, 1687–1692.

[14] V. M. Zamarion, R. A. Timm, K. Araki, H. E. Toma, *Inorg. Chem.* **2008**, *47*, 2934–2936.

[15] K. Araki, E. Mizuguchi, H. Tanaka, T. Ogawa, *J. Nanosci. Nanotechnol.* **2006**, *6*, 708–712.

[16] S. K. Ghosh, T. Pal, *Chem. Rev.* **2007**, *107*, 4797–4862.

[17] I. E. Sendroiu, S. F. L. Mertens, D. J. Schiffrin, *Phys. Chem. Chem. Phys.* **2006**, *8*, 1430–1436.

[18] a) K. Araki, M. J. Wagner, M. S. Wrighton, *Langmuir* **1996**, *12*, 5393–5398; b) H. E. Toma, K. Araki, *Coord. Chem. Rev.* **2000**, *196*, 307–329.

[19] A. Maier, A. R. Rabindranath, B. Tieke, *Chem. Mater.* **2009**, *21*, 3668–3676.

[20] a) W. Pan, C. J. Durning, N. J. Turro, *Langmuir* **1996**, *12*, 4469–4473; b) K. Hu, A. J. Bard, *Langmuir* **1998**, *14*, 4790–4794; c) C. D. Bain, E. B. Troughton, Y. T. Tao, J. Evall, G. M. Whitesides, R. G. Nuzzo, *J. Am. Chem. Soc.* **1989**, *111*, 321–335; d) J. I. Henderson, S. Feng, G. M. Ferrence, T. Bein, C. P. Kubiak, *Inorg. Chim. Acta* **1996**, *242*, 115–124.

[21] F. S. Damos, R. C. S. Luz, L. T. Kubota, *Langmuir* **2005**, *21*, 602–609.

[22] T. M. Willey, A. L. Vance, T. van Buuren, C. Bostedt, A. J. Nelson, L. J. Terminello, C. S. Fadley, *Langmuir* **2004**, *20*, 2746–2752.

[23] a) C. E. D. Chidsey, D. N. Loiacono, *Langmuir* **1990**, *6*, 682–691; b) O. Dannenberger, K. Weiss, H. J. Himmel, B. Jager, M. Buck, C. Woll, *Thin Solid Films* **1997**, *307*, 183–191.

[24] Z. P. Zhuang, J. B. Cheng, H. Y. Jia, J. B. Zeng, X. X. Han, B. Zhao, H. X. Zhang, G. Zhang, W. Zhao, *Vib. Spectrosc.* **2007**, *43*, 306–312.

[25] Y. Tufan, N. Karacan, *J. Inclusion Phenom. Mol. Recognit. Chem.* **1997**, *27*, 193–200.

[26] a) H. E. Toma, C. Cipriano, *Monatsh. Chem.* **1989**, *120*, 815–820; b) H. E. Toma, P. S. Santos, C. Cipriano, *Spectrosc. Lett.* **1988**, *21*, 909–918; c) M. K. Johnson, D. B. Powell, R. D. Cannon, *Spectrochim. Acta Part A* **1981**, *37*, 995–1006.

[27] J. B. Cheng, X. L. Li, W. Song, W. Q. Xu, B. Zhao, G. Zhang, *Chem. Phys. Lett.* **2005**, *405*, 344–351.

[28] K. Nakamoto, *Infrared and Raman spectra of inorganic and coordination compounds*, 5th ed., Wiley, New York, **1997**.

[29] a) F. Cunha, N. J. Tao, X. W. Wang, Q. Jin, B. Duong, J. DAgnese, *Langmuir* **1996**, *12*, 6410–6418; b) T. Wandlowski, K. Ataka, D. Mayer, *Langmuir* **2002**, *18*, 4331–4341.

[30] B. Q. Xu, N. J. J. Tao, *Science* **2003**, *301*, 1221–1223.

[31] Q. X. Lia, X. J. Wu, J. Huang, J. L. Yang, *Ultramicroscopy* **2005**, *105*, 293–298.

[32] a) J. C. Rubim, *J. Electroanal. Chem.* **1987**, *220*, 339–350; b) C. S. Allen, R. P. Vanduyne, *Chem. Phys. Lett.* **1979**, *63*, 455–459.

[33] O. Pluchery, W. Q. Zheng, T. Marin, A. Tadjeddine, *Phys. Status Solidi A* **1999**, *175*, 145–151.

[34] M. Tadjeddine, J. P. Flament, *Chem. Phys.* **2001**, *265*, 27–46.

[35] C. M. Coyle, G. Chumanov, P. W. Jagodzinski, *J. Raman Spectrosc.* **1998**, *29*, 757–762.

[36] a) P. Wang, Z. B. Mai, Z. Dai, Y. X. Li, X. Y. Zou, *Biosens. Bioelectron.* **2009**, *24*, 3242–3247; b) X. Huang, Y. X. Li, Y. L. Chen, L. Wang, *Sens. Actuators, B* **2008**, *134*, 780–786; c) E. V. Milsom, J. Novak, M. Oyama, F. Marken, *Electrochem. Commun.* **2007**, *9*, 436–442.

[37] M. Itou, M. Otake, Y. Araki, O. Ito, H. Kido, *Inorg. Chem.* **2005**, *44*, 1580–1587.

[38] J. Turkevich, P. C. Stevenson, J. Hillier, *Discuss. Faraday Soc.* **1951**, 55.

Received: October 19, 2010
Published Online: February 17, 2011

